## SSDM2024-121556

# PROGRESSIVE DAMAGE ANALYSIS OF CURVED COMPOSITE LAMINATES INCORPORATING EFFECTS OF MANUFACTURING USING A SEMI-DISCRETE DAMAGE MODEL

Sai Krishna Meka<sup>1</sup>, Ryan Enos<sup>1</sup>, James Roach<sup>2</sup>, Dianyun Zhang<sup>1,\*</sup>

<sup>1</sup>Purdue University, West Lafayette, IN <sup>2</sup>University of Connecticut, Storrs, CT

## **ABSTRACT**

This study underscores the remarkable strength-to-weight advantage offered by curved composite laminates in comparison to conventional materials like metal, preserving or even surpassing strength levels. To comprehensively assess the strength characteristics of such laminates, the research delves into the primary failure modes governing their out-of-plane strength, predominantly matrix failure and delamination. It is essential to consider the impact of manufacturing processes, which introduce residual stresses and spring-in phenomena.

To address these complexities, a finite element simulation is employed, integrating manufacturing effects and adopting a semi-discrete damage model. Within this model, matrix failure within the plies is delineated using a smeared crack approach, whereby crack directionality aligns passively with fiber orientation within each ply. Furthermore, the smeared crack approach is extended to model damage occurring at ply interfaces.

This comprehensive investigation is done for the layup sequence:  $[45^{\circ}/0^{\circ}/-45^{\circ}/90^{\circ}]_{3S}$  - symmetric and balanced laminate. Experimental validation is achieved through a 4-point bending test by adhering close to ASTM D6415 standards, gauging the curved beam strength/inter-laminar strength of fiber-reinforced polymer matrix composites. The utilization of DIC images aids in the systematic observation and comprehension of failure modes across various scenarios.

## Keywords: Cure Kinetics, CHILE, Smeared Crack Approach, four point bending, delamination, failure, L beam

## **NOMENCLATURE**

 $\mathbf{D}^{co}$  Continuum Stiffness  $[ML^{-1}T^{-2}]$   $\mathbf{D}^{cr}$  Unloading Stiffness  $[ML^{-1}T^{-2}]$   $\mathbf{D}^{da}$  Damping matrix  $[ML^{-1}T^{-1}]$ N Transformation Matrix

 $e^{cr}$  Crack strain in crack coordinate system  $s^{cr}$  Crack stress in crack coordinate system

\*Corresponding author: dianyun@purdue.edu

L Characteristic Length [L]  $\sigma$  Total Stress [ $ML^{-1}T^{-2}$ ]

 $\varepsilon$  Total strain

 $\varepsilon^{co}$  Continuum strain

 $\varepsilon^{cr}$  Crack strain

 $arepsilon^{el}$  Elastic strain

 $\varepsilon^{pl}$  Plastic strain

 $\varepsilon_{nn}^{cr}$  local critical strain in the normal direction  $E_1$  Longitudinal Young's modulus of Lamina

 $v_{12}$  In-plane Poisson's ratio of Lamina

K<sub>23</sub> Bulk modulus of Lamina

 $G_{12}$  In-plane shear modulus of Lamina

 $G_{23}$  Out-of-plane shear modulus of Lamina

 $E^m$  Young's modulus of matrix

 $G^m$  Shear modulus of matrix

 $K_{22}^m$  Bulk modulus of matrix

 $V_f^2$  Volume fraction of lamina (between 0 to 1)

 $E_X, E_Y$  Effective Young's modulii of Laminate

 $v_{XY}$  Effective Poisson's ratio of Laminate

 $G_{XY}$  Effective in-plane shear modulus of Laminate

b Degree of cure of matrix

 $\phi_{gel}$  Degree of cure of matrix at the gelation point

m, n, C, A Cure kinetics constants

T Temperature

 $\Delta E$  Activation energy

 $a_i$  (i=1 to 7) Cure kinetic constants modified

### 1. INTRODUCTION

The four point bending test is a common method used to evaluate the mechanical properties of composite materials. This test is performed to assess the inter-laminar strength and observe the delamination failure in the composite beam. The four point bending test is a versatile and widely used method for characterizing the mechanical behavior of composite materials, providing crucial information for material selection, design, and quality assurance in various engineering applications.

In this particular study we investigate the composite beam with layup sequence:  $[45^{\circ}/0^{\circ}/-45^{\circ}/90^{\circ}]_{3S}$  which happens to be

a symmetric and balanced laminate. Due to which, the mechanical properties in the through thickness direction are uniform, and there are minimized shear effects on the laminate.

From a modeling standpoint, to study delamination in the FEA models, cohesive zone is modeled between plies in the composite part. However, cohesive zone models often require various material parameters, including the cohesive strength, critical energy release rate, and shape of the traction-separation law. Determining these parameters experimentally can be challenging and may lead to inaccuracies in the simulation results. Accurately calibrating the cohesive zone model parameters to match experimental data can be difficult. Inaccurate parameters can lead to poor predictions of crack propagation and failure. Cohesive zone modeling typically involves more computational effort than simpler fracture models. Simulating large and complex structures with cohesive zone models can be computationally expensive and time-consuming.

Instead, we employ the continuum damage method called the "Smeared Crack Approach (SCA)" to model the through thickness damage as well as in plane damage. We further intend to incorporate the effects of manufacturing process i.e. take into account the residual stresses developed in the composite part due to manufacturing process and perform an "incremental" smeared crack approach.

## 2. FINITE ELEMENT MODELING

The finite element modeling strategy is to model the composite part and tool (mold) and then have a heat transfer analysis that simulates the manufacturing process of curing the composite part in an autoclave on a mold. We also run an analysis that simulates the removal of the part from the mold such that the spring in angle is obtained through the analysis while there is residual stress development in the composite part.

The part model on which we intend to carry out the damage simulation is as shown in the figure 1.

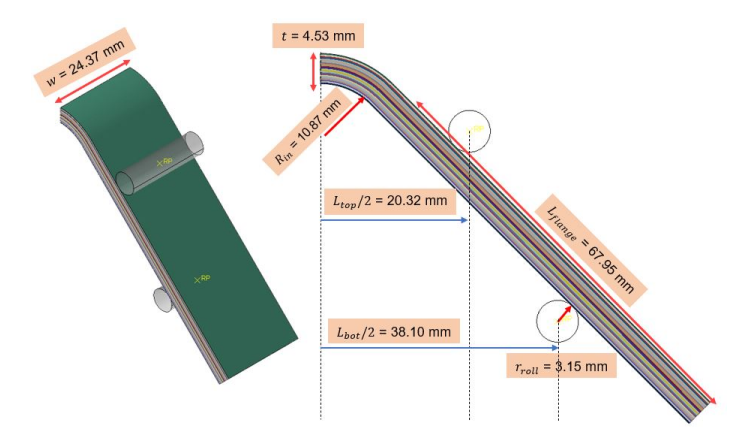


FIGURE 1: SCHEMATIC OF DISCRETE LAMINATE MODEL IN WHICH EACH PLY IS MODELED

We employ two models for the finite element modeling. In one model (*homogenized model*) we homogenize the material properties by computing the effective laminate properties using CLPT (Classical Laminate Plate Theory) and assign it to the part. In the other model (*discrete model*) we model each ply by

partitioning the laminate (figure 1) and assign each of the plies the lamina properties that we compute using CCA (Composite Cylinder Assemblage) (??). We assign the plies appropriate material orientation based on the layup sequence specified.

The simulations on both the models are performed assuming the composite material to be elastic and assuming no initiation of damage to observe the deviation between the results of both the models. So we can comment on the accuracy of CLPT and find out whether it would be justified to use the homogenized model over the discrete model.

The total force on the rollers vs displacement of each roller for both the homogenized and discrete models is plotted as shown in figure 2.

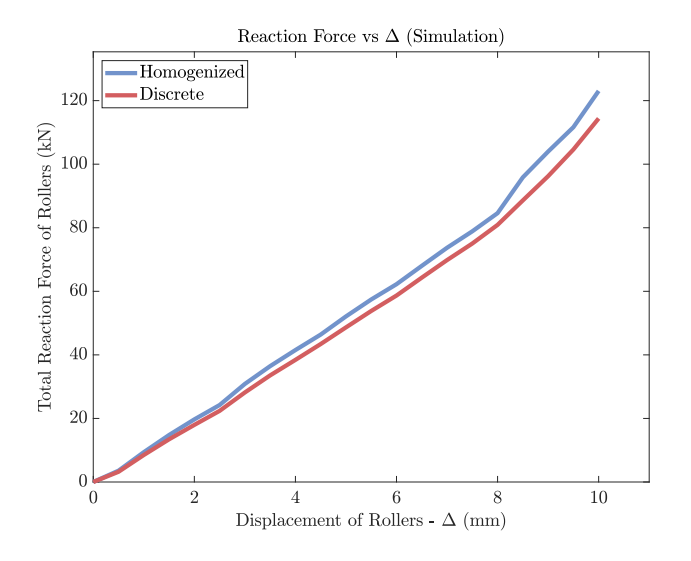


FIGURE 2: FORCE VS DISPLACEMENT OF THE ROLLERS FOR HO-MOGENIZED MODEL AND DISCRETE MODEL

The true and approximate inter-laminar strengths are computed using solutions that were developed by Lekhnitskii and provided in the ASTM D6415/D6415M standard. The plot of inter-laminar strengths vs the displacement of the rollers for the simulations are as shown in the figure 3.

We observe that the results for both the *discrete* model and the *homogenized* model are very close to each other so it would suffice to investigate the homogenized model if we intend to understand the elastic behavior of the composite part.

### 3. CONSTITUTIVE MODEL

To incorporate the damage aspect in the model we adopt the concept of Smeared Crack Approach (SCA) [1]. In SCA, the effect of the micro-cracks are smeared over a characteristic length as shown in figure 5. This smearing effect is mathematically characterized by deteriorating the secant stiffness of the material as the damage progresses once the transition criteria (i.e. failure criteria) is satisfied. Here, we use the 'Maximum stress failure' criterion.

When the local stresses reach the critical strength value, we conclude that failure has initiated and the material transitions

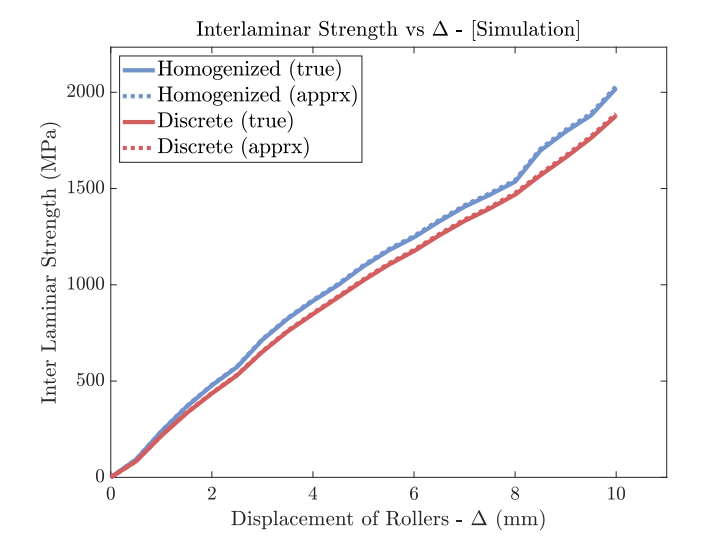


FIGURE 3: INTER-LAMINAR STRENGTHS VS DISPLACEMENT OF THE ROLLERS FOR *HOMOGENIZED* MODEL AND *DISCRETE* MODEL

from pre-peak behavior to post-peak behavior. The pre-peak behavior corresponds to the matrix micro damage due to the growth of voids and flaws in the matrix, while the post-peak behavior corresponds to the accumulation of matrix micro damage which leads to matrix macroscopic cracking [1]. The pre-peak behavior is governed by a linear elastic constitutive law, i.e., a strain-based formulation. While in the post-peak regime the softening of the material is captured by a displacement-based formulation of linear traction-separation law as show in figure 4.

Before we formulate the damage model constitutive law, we need to first compute the effective lamina/laminate properties for which we will have to employ CCA and CLPT respectively.

## 3.1 Computing effective lamina and laminate properties

CCA formulation proposed by Hashin and Rosen [3] is used to model the mechanical behavior of the composite lamina. We have the fiber (IM7) and matrix (8552) properties from the tables 3 and 4 from which we can compute the lamina properties using equations in 1 to 5 listed below.

$$E_1 = E_1^f V_f + E^m (1 - V_f) + \frac{4V_f (1 - V_f)(v_{12}^f - v^m)^2 G^m}{\frac{G^m (1 - V_f)}{K_{23}^f} + \frac{G^m V_f}{K_{23}^m} + 1}$$
(1)

$$v_{12} = v_{12}^{f} V_f + v^m (1 - V_f) + \frac{V_f (1 - V_f) (v_{12}^{f} - v^m) \left( \frac{G^m}{K_{23}^m} - \frac{G^m}{K_{23}^f} \right)}{\frac{G^m (1 - V_f)}{K_{23}^f} + \frac{G^m V_f}{K_{23}^m} + 1}$$
(2)

$$K_{23} = K_{23}^m + \frac{V_f}{\frac{1}{K_{23}^f - K_{23}^m} + \frac{1 - V_f}{K_{23}^m + G^m}}$$
(3)

$$G_{12} = G^m \left( \frac{G_{12}^f (1 + V_f) + G^m (1 - V_f)}{G_{12}^f (1 - V_f) + G^m (1 + V_f)} \right)$$
(4)

$$G_{23} = G^m \left[ 1 + \frac{V_f}{G^m + \frac{(K_{23}^m + 2G^m)(1 - V_f)}{2(K_{23}^m + G^m)}} \right]$$
 (5)

To find the effective properties of the entire composite laminate we use CLPT (Classical Laminate Plate Theory) based on the layup of the composite and its thickness information. We have investigated the composite laminate with layup  $[45^{\circ}/0^{\circ}/-45^{\circ}/90^{\circ}]_{3S}$  and thickness 4.53 mm in this study. The volume fraction of the composite is 50%. The effective lamina properties computed using CCA are listed in table 1.

Effective Lamina Properties		
	(computed using CCA)	
Quantity	Description	Value
$\overline{E_1}$	Longitudinal Young's Modulus	140.52 GPa
$E_2 = E_3$	Transverse Young's Modulus	9.34 GPa
$v_{12} = v_{13}$	In-plane poisson's ratio	0.18
$v_{23}$	Out-of-plane poisson's ratio	0.59
$G_{12} = G_{13}$	In-plane Shear Modulus	4.80 GPa
$G_{23}$	Out-of-plane Shear Modulus	2.93 GPa

TABLE 1: EFFECTIVE LAMINA PROPERTIES OF IM7/8552 LAMINA WITH A VOLUME FRACTION OF 50%

The composite laminate is symmetric and balanced as we can observe from the layup sequence. The effective laminate properties using CLPT are computed and listed in table 2

Effective Laminate Properties (computed using CLPT)		
Quantity	Description	Value
$E_X = E_Y$	Young's Modulus	53.88 GPa
$ u_{XY}$	Poisson's ratio	0.29
$G_{XY}$	Shear Modulus	20.75 GPa

TABLE 2: EFFECTIVE LAMINATE PROPERTIES OF A  $[45/0/-45/90]_{3S}$  IM7/8552 COMPOSITE

#### 3.2 SCA formulation

In the pre-peak regime, standard continuum descriptions of the material are assumed to hold. In the post-peak regime, it is assumed that the total strain  $\varepsilon$  may be split up into a continuum part and a crack part.

$$\varepsilon = \begin{cases} \varepsilon^{co} & \text{in pre-peak regime} \\ \varepsilon^{co} + \varepsilon^{cr} & \text{in post-peak regime} \end{cases}$$
 (6)

 $arepsilon^{co}$  is the continuum strain which can be further decomposed into

$$\varepsilon^{co} = \varepsilon^{el} + \varepsilon^{pl} + \varepsilon^{th} \tag{7}$$

Where  $\varepsilon^{el}$  is the elastic strain,  $\varepsilon^{pl}$  is the plastic strain, and  $\varepsilon^{th}$  is the thermal strain. For our study the plastic strain is neglected.

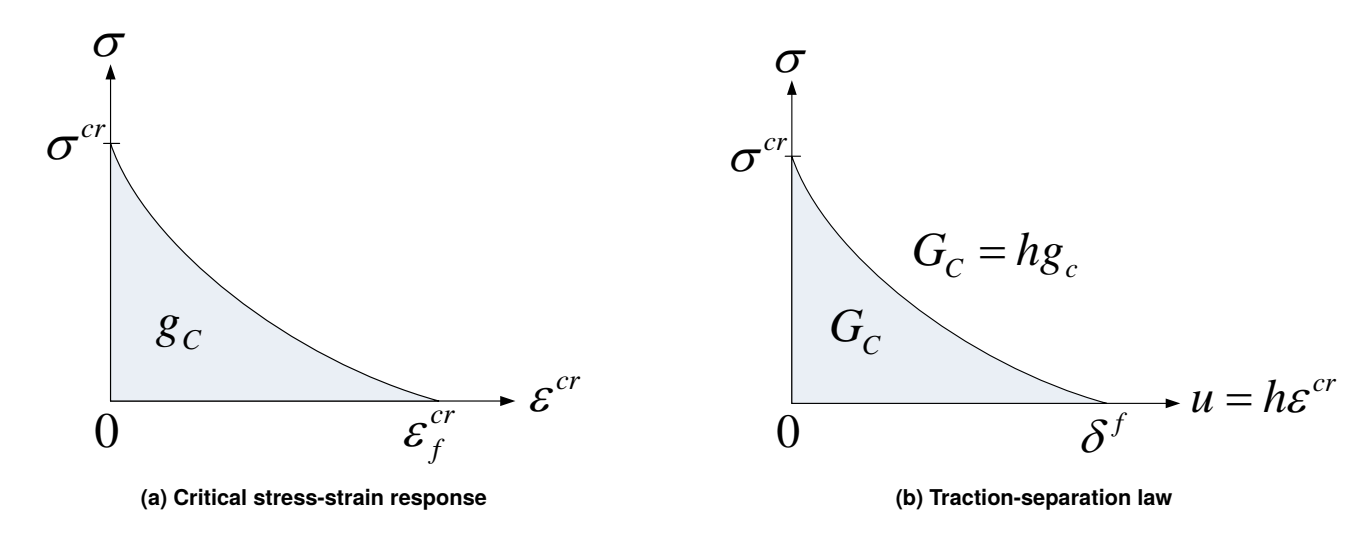


FIGURE 4: STRESS-STRAIN SOFTENING RESPONSE IS RELATED TO THE TRACTION-SEPARATION LAW THROUGH A CHARACTERISTIC LENGTH. [2]

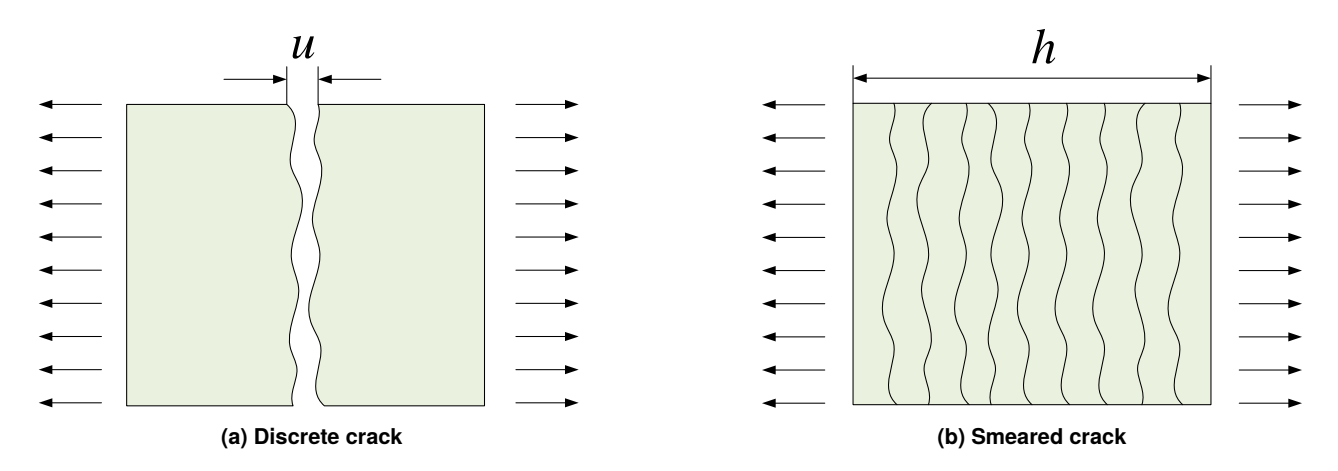


FIGURE 5: DISCRETE CRACKS SMEARED WITHIN A FINITE ELEMENT [2]

Then the total strain can be written as

$$\Delta \varepsilon = \begin{cases} \Delta \varepsilon^{el} + \Delta \varepsilon^{th} & \text{in pre-peak regime} \\ \Delta \varepsilon^{el} + \Delta \varepsilon^{th} + \Delta \varepsilon^{cr} & \text{in post-peak regime} \end{cases}$$
(8)

The relation between the local crack strains and the global crack strains is

$$\Delta \varepsilon^{cr} = N \Delta e^{cr} = N \begin{bmatrix} \Delta \varepsilon_{nn}^{cr} \\ \Delta \gamma_{t1}^{cr} \\ \Delta \gamma_{t2}^{cr} \end{bmatrix}. \tag{9}$$

Where 'N' is the transformation matrix (See Appendix A of [2] for the derivation of N).

Similarly, the incremental global stress ( $\Delta \sigma$ ) can be transformed to yield the incremental tractions at the crack interface  $(\Delta s^{cr})$  as follows -

$$\Delta s^{cr} = \begin{bmatrix} \Delta \sigma_{nn}^{cr} \\ \Delta \tau_{t1}^{cr} \\ \Delta \tau_{t2}^{cr} \end{bmatrix} = N^T \Delta \sigma.$$

The incremental tractions at the crack interface ( $\Delta s^{cr}$ ) are related to the incremental crack strain ( $\Delta e^{cr}$ ) through the secant stiffness matrix  $(D^{cr})$  and a damping matrix  $(D^{da})$  by

$$\Delta s^{cr} = D^{cr} \Delta e^{cr} + D^{da} \Delta \dot{e}^{cr}.$$

The damping matrix makes the crack progression a timedependent property. This can also be used to smoothen the numerical solution scheme. Any numerical scheme involves a discrete time step. The crack strain rate is accordingly approximated with finite differences as

$$\Delta \dot{\mathbf{e}}^{cr} \approx \frac{\Delta e^{cr}(t+\Delta t) - \Delta e^{cr}(t)}{\Delta t} = \frac{\Delta e^{cr} - \Delta e^{cr}_{old}}{\Delta t}.$$

The relation between the total stress (global) i.e. " $\Delta \sigma$ " and the elastic strain i.e. " $\Delta \varepsilon$ " is based on Hooke's law as follows

$$\Delta \sigma = D^{co} \Delta \varepsilon^{el}.$$

Where  $D^{co}$  is the continuum stiffness matrix, given by  $(S^{co})^{-1}$  and  $S^{co}$  is compliance matrix given as follows for a transversely isotropic material:

$$S^{co} = \begin{bmatrix} \frac{1}{E_1} & \frac{-\nu_{12}}{E_1} & \frac{-\nu_{12}}{E_1} & 0 & 0 & 0 \\ -\frac{\nu_{12}}{E_1} & \frac{1}{E_2} & -\frac{\nu_{23}}{E_2} & 0 & 0 & 0 \\ -\frac{\nu_{12}}{E_1} & -\frac{\nu_{23}}{E_2} & \frac{1}{E_2} & 0 & 0 & 0 \\ 0 & 0 & 0 & \frac{1}{G_{12}} & 0 & 0 \\ 0 & 0 & 0 & 0 & \frac{1}{G_{12}} & 0 \\ 0 & 0 & 0 & 0 & 0 & \frac{2(1+\nu_{23})}{E_2} \end{bmatrix}$$

Note: 
$$G_{23} = \frac{E_2}{2(1 + v_{23})}$$

Combining all equations results in an implicit relation between the crack strain and the total elastic strain. Finally, the relation between incremental stress and incremental strain in the post-peak regime is formulated.

## 3.3 Integrating manufacturing effects

The curing process in the composite processing model involves multiple physical phenomena such as resin cure kinetics, chemical shrinkage, and thermal loading. In order to predict curing induces residual stresses we employ the modeling framework developed in [4]. According to [4] for an epoxy resin such as EPON 8552, the cure kinetics relation can be expressed using the Kamal-Souror autocatalytic + diffusion model as

$$\dot{\phi}(\phi, T) = \frac{k(T)\phi^{m}(1 - \phi)^{n}}{1 + exp[C(\phi - \phi_{gel}(T))]}$$
(10)

Where  $k(T) = Aexp(-\triangle E/(RT))$ .

Equation 10 be re-written in a parametric form as follows

$$\dot{\phi}(\phi, T, a) = \frac{a_1 exp(-a_2/(RT))\phi^{a_3}(1-\phi)^{a_4}}{1 + exp(a_5(\phi - a_6 - a_7T))}.$$
 (11)

The values of these cure kinetics parameters for EPON 8552 are listed in table 6.

In the pre-gelation stage the resin is in the liquid state and there are no stresses developed. As the gelation point occurs in the cure cycle the resin becomes rubbery, the Young's modulus and the thermal expansion coefficient of the resin change to  $E_{rubber}^{m}$ and  $\alpha^{rubber}$  respectively. The constitutive relation during the rubbery state is hence given as

$$\triangle \sigma = C_R (\triangle \varepsilon - \alpha^{rubber} \triangle T - \triangle \varepsilon^{ch})$$

Where  $C_R$  is the stiffness matrix calculated for the isotropic matrix whose Young's Modulus is  $E^m_{rubber}$  and Poisson's ratio is  $v^m_{rubber}$  (for this particular material it so happens that the Poisson's ratio in both the rubbery and glassy state are almost the same i.e.,  $v_{rubber}^m = v_{glass}^m$ ) Similarly, in the Glassy state the constitutive law modifies to

$$\Delta \sigma = C_G(\Delta \varepsilon - \alpha^{glass} \Delta T - \Delta \varepsilon^{ch}).$$

Where  $C_G$  is the stiffness matrix calculated for the isotropic matrix whose Young's Modulus and Poisson's ratio are  $E_{glass}^{m}$ and  $v_{glass}^m$  respectively.

#### 4. EXPERIMENT DETAILS

The composite part used in the experiments is made using prepregs of IM7/8552 cured using autoclave. The layup sequence of the composite laminate is  $[+45^{\circ}/0^{\circ}/-45^{\circ}/90^{\circ}]_{3S}$  which is a symmetric and balanced laminate. The material properties of IM7 (fiber) are listed in table 3 and the properties of EPON 8552 are listed in tables 4, 5 and 6.

The four point bending experiment setup looks as shown in the figure 6, where the bottom fixture is allowed to move during **IM7** (Fiber Properties)

IWI7 (Fiber Properties)		
Symbol	Description	Value
$E_1^f$	Longitudinal Young's modulus	276000 MPa
$E_2^f$	Transverse Young's Modulus	19500 MPa
$v_{12}^{\overline{f}}$	In-plane Poisson's ratio	0.01978 MPa
$E_{2}^{f} \ v_{12}^{f} \ G_{23}^{f}$	In-plane shear modulus	70000 MPa
$G_{23}^{f}$	Out of plane shear modulus	5735 MPa
$\alpha_1^f$	Longitudinal thermal expansion coefficient	$-4 * 10^{-7} \text{ K}^{-1}$
$lpha_2^f$	Transverse thermal expansion coefficient	$5.6 * 10^{-6} \text{ K}^{-1}$
$ ho^f$	Density	$1.8 \text{ g/cm}^3$
$\begin{matrix} \rho^f \\ C_P^f \end{matrix}$	Specific heat	1.13 J/gK
$K_1^f$	Longitudinal thermal conductivity	6.83 W/mK
$K_2^f$	Transverse thermal conductivity	2.18 W/mK

**TABLE 3: IM7 FIBER PROPERTIES** 

8552 Epoxy Matrix Properties - Mechanical		
Symbol	Description	Value
$E_{glass}^{m}$	Resin Young's Modulus (Glassy State)	4670 MPa
$v_{glass}^{m}$	Poisson's ratio (Glassy State)	0.37
$\phi_{gel}$	Degree of cure  @ gel point	0.43
$E^m_{rubber}$	Resin Young's Modulus (Rubbery State)	46.7 MPa
vshtm	Resin volumetric shrinkage	-0.0494
$\alpha^{rubber}$	Thermal expansion coefficient (Rubbery State) $18.2 * 10^{-5}$	
$\alpha^{glass}$	Thermal expansion coefficient (Glassy State)	$5 * 10^{-5} \text{ K}^{-1}$
λ	Coefficient in the Debenedetto equation	0.78
$T_{g_{_{\!\scriptscriptstyle L}}}^0$	$T_g$ of the uncured resin 265.15 K	
$T_{g}^{f}$	$T_g$ of the fully cured resin	523.15 K

TABLE 4: 8552 EPOXY MATRIX PROPERTIES - MECHANICAL

85	552 Epoxy Matrix Properties -	Thermal	
Symbol	Description	Value	
$\rho^m$	Resin density	1.2 g/cm <sup>3</sup>	
$Cp00^m$	Resin specific heat at $\phi = 0$ & T = 273.15 K		
$Cp10^m$	Resin specific heat at $\phi = 1$ & T = 273.15 K		
$Cp0^m_{TEMP}$	Resin specific heat per T @ $\phi = 0$ 2.77 * $10^{-3}$ J		
$Cp1_{TEMP}^{m}$	Resin specific heat per T $@ \phi = 1$	$3.34 * 10^{-3} \text{ J/gK}^2$	
$K_{00}^m$	Resin thermal conductivity at $\phi = 0 \& T = 273.15 \text{ K}$	0.148 W/mK	
$K_{10}^{m}$	Resin thermal conductivity at $\phi = 1 \& T = 273.15 \text{ K}$	0.188 W/mK	
$K0^m_{TEMP}$	Resin thermal conductivity per T @ $\phi = 0$	0 W/mK	
$K1_{TEMP}^{m}$	Resin thermal conductivity per T @ $\phi = 1$	0.0007 W/mK	

**TABLE 5: 8552 EPOXY MATRIX PROPERTIES - THERMAL** 

8552 Epoxy Matrix - Cure Kinetics Properties		
Parameter	Value	
$a_1$	$1.53*10^5$	
$a_2$	$6.65 * 10^4$	
$a_3$	0.813	
$a_4$	2.74	
$a_5$	43.1	
$a_6$	-1.684	
$a_7$	$5.46 * 10^{-3}$	

TABLE 6: CURE KINETICS PARAMETERS OF 8552 EPOXY MATRIX

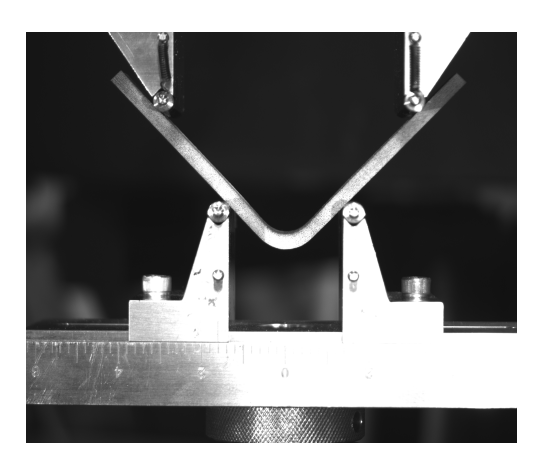


FIGURE 6: FOUR POINT BENDING EXPERIMENT SETUP

the testing which acts as the load while the top fixture is not allowed to move.

We observe delamination mode of failure in the laminate as we load the specimen which can be seen in the figure 7.

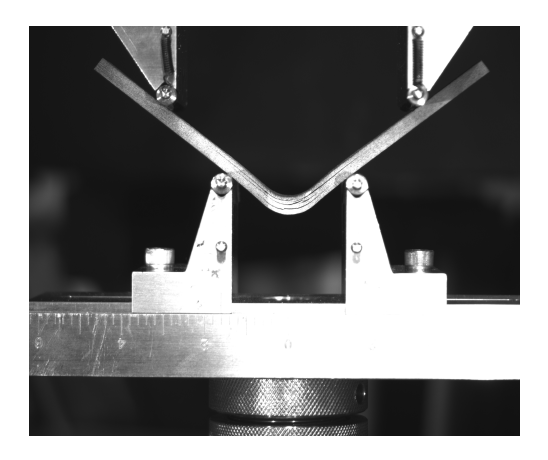


FIGURE 7: DELAMINATION FAILURE IN THE IM7/8552 LAMINATE

The force vs displacement of the rollers graph is as shown in figure 8.

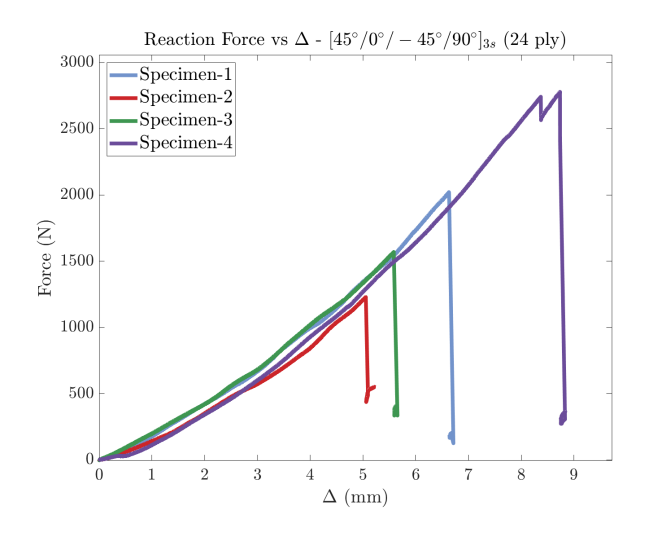


FIGURE 8: FORCE VS DISPLACEMENT OF THE ROLLERS FOR THE EXPERIMENTALLY TESTED SPECIMENS

The true interlaminar strengths are computed using solutions that were developed by Lekhnitskii and provided in the ASTM D6415/D6415M standard. These inter-laminar strengths vs displacement of the rollers are plotted in figure 9.

#### 5. RESULTS AND DISCUSSION

Comparison of the simulation results where the damage model is employed for a homogenized laminate with experimental results shows that the trend of both experiments and simulation is the same. However, the pre-peak slope of the simulation curve is higher than what we observe for the experiment specimens as shown in figure 10.

The reason for this could be the fact that the moving parts in the MTS machine in which the experiment is conducted could add

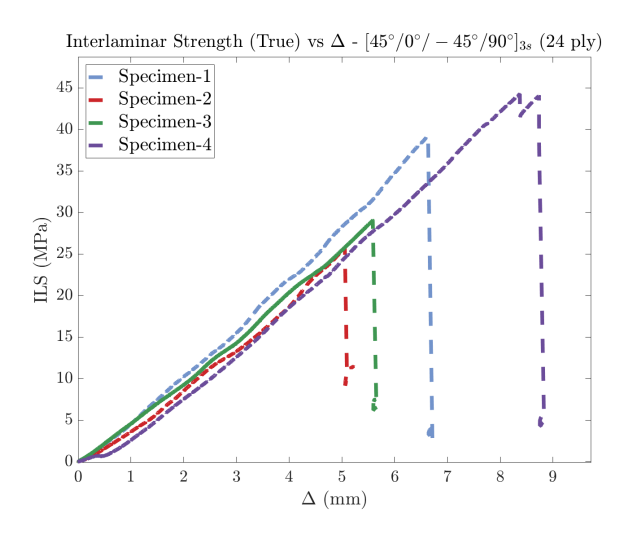


FIGURE 9: INTER-LAMINAR STRENGTH VS DISPLACEMENT OF THE ROLLERS FOR THE EXPERIMENTALLY TESTED SPECIMENS

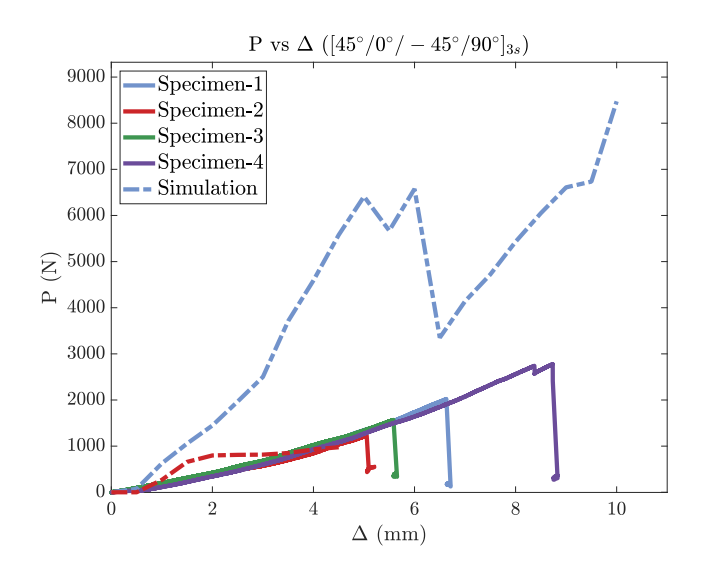


FIGURE 10: COMPARISON OF FORCE VS DISPLACEMENT OF THE ROLLERS FOR THE EXPERIMENTALLY TESTED SPECIMENS AND THE HOMOGENIZED SIMULATION MODEL

compliance to the system. Another reason could be the age of the prepreg material used to manufacture the laminate. The stiffness values of older prepregs are generally around 25% lesser than what they are expected to have as prescribed by the manufacturer. The culmination of these two possibilities could have lead to the decline in the pre-peak slopes of the experimental specimens.

From the modeling aspect the complexities arise based on our choice of the contact conditions for the rollers and the laminate. This needs to be done by trying various possibilities and comparing it with a benchmark solution for a known problem such as a three-point bending experiment of a flat plate laminate.

Further study has to be done on the implementation of damage model in a discretized model having fiber aligned meshes. We aim to conduct more reliable experiments with newer prepregs and verify the simulation results with the new batch of data that we acquire.

#### **ACKNOWLEDGMENTS**

We would like to express my sincere gratitude to the National Science Foundation (NSF) for their generous financial support, which made this research possible. Their commitment to advancing scientific knowledge and fostering innovative research has been instrumental in the success of this project.

I am deeply thankful for the NSF grant no. 2105448 that provided the necessary funding to conduct the experiments, analyze the data, and disseminate the findings. This support not only contributed to the advancement of our understanding in our research, but also facilitated the development of critical skills and expertise among the research team.

### **REFERENCES**

[1] Bažant, Zdeněk P and Oh, Byung H. "Crack band theory for fracture of concrete." *Matériaux et construction* Vol. 16

- No. 3 (1983): pp. 155–177.
- [2] Zhang, Dianyun, Waas, Anthony M. and Yen, Chian-Fong. "Progressive damage and failure response of hybrid 3D textile composites subjected to flexural loading, part II: Mechanics based multiscale computational modeling of progressive damage and failure." *International Journal of Solids and Structures* Vol. 75-76 (2015): pp. 321–335.
- [3] Hashin, Z. and Shtrikman, S. "On some variational principles in anisotropic and nonhomogeneous elasticity." *Journal of the Mechanics and Physics of Solids* Vol. 10 No. 4 (1962): pp. 335–342. DOI https://doi.org/10.1016/0022-5096(62)90004-2.
- [4] Zhou, Kai, Enos, Ryan, Zhang, Dianyun and Tang, Jiong. "Uncertainty analysis of curing-induced dimensional variability of composite structures utilizing physics-guided Gaussian process meta-modeling." *Composite Structures* Vol. 280 (2022): p. 114816.
- [5] Bogetti, Travis A and Gillespie Jr, John W. "Process-induced stress and deformation in thick-section thermoset composite laminates." *Journal of composite materials* Vol. 26 No. 5 (1992): pp. 626–660.
- [6] Heinrich, Christian and Waas, Anthony. "Investigation of progressive damage and fracture in laminated composites using the smeared crack approach." 53rd AIAA/ASME/ASCE/AHS/ASC Structures, Structural Dynamics and Materials Conference 20th AIAA/ASME/AHS Adaptive Structures Conference 14th AIAA: p. 1537. 2012.